Article

Effect of Y_2O_3 on the Electrical Contact Behavior of Al_2O_3-Cu/MoTa Composites

Yunzhang Li [1], Meng Zhou [1,2,3,*], Yi Zhang [1,2,3,*], Hanjing Zhu [1], Xianhua Zheng [1], Shengli Liang [1], Shunlong Tang [1], Baohong Tian [1,2,3], Yong Liu [1,2,3], Xu Li [4], Alex A. Volinsky [5] and Chenglin Zheng [1]

1 School of Materials Science and Engineering, Henan University of Science and Technology, Luoyang 471023, China
2 Provincial and Ministerial Co-Construction of Collaborative Innovation Center for Non-Ferrous Metals New Materials and Advanced Processing Technology, Luoyang 471023, China
3 Henan Province Key Laboratory of Nonferrous Materials Science and Processing Technology, Luoyang 471023, China
4 Center for Advanced Measurement Science, National Institute of Metrology, Beijing 100029, China
5 Department of Mechanical Engineering, University of South Florida, 4202 E. Fowler Ave. ENG 030, Tampa, FL 33620, USA
* Correspondence: zhoumeng0902@126.com (M.Z.); yizhang@haust.edu.cn (Y.Z.)

Abstract: With the massive penetration of electronics into human life, higher demands are placed on electrical contacts. Among them, the lifetime of electrical contacts and safety are the most concerning. In this research, Al_2O_3-Cu/25Mo5Ta and $0.5Y_2O_3/Al_2O_3$-Cu/25Mo5Ta composites were prepared by using ball milling and powder metallurgy methods. The two composites were subjected to 10,000 contact opening and closing electrical contact experiments and the arc duration and arc energy were analyzed. The results show that the addition of Y_2O_3 has a slight effect on the mechanical properties of the Al_2O_3-Cu/25Mo5Ta composites but has a significant effect on the electrical contact performance. Y_2O_3 can reduce the mass loss of the electrical contacts during the electrical contact process, which prolongs their service life. The addition of Y_2O_3 decreased the average arc duration and arc energy of the electrical contact material by 21.53% and 18.02%, respectively, under the experimental conditions of DC 30 V, 10 A. TEM results showed that nanoscale $YTaO_4$ with excellent thermal stability was generated during the sintering process, which has a positive effect on the electrical contact performance of the composites.

Keywords: copper matrix composites; electrical contact; arc erosion behavior; yttrium tantalate

1. Introduction

Circuits are indispensable in industries such as electronics, information, aerospace and other fields. In the circuit, the electrical contacts play a crucial role in controlling the opening and closing of the switch, and the regular operation of various original components is affected by the electrical contact material. The stability of the electrical contact material in the process of electrical contact determines the operation of electronic devices and is a vital part of electrical safety. With the massive penetration of electronics into human life, higher demands have been placed on electrical contacts [1,2]. Among them, the lifetime of electrical contacts and safety are the most concerning. The arc line contraction and voltage drop will cause a steep increase in Joule heat generated in the contact area, causing the contact surface of the electrical contacts to melt slightly. This is because the contact between electrical contacts during electrical contact is made by conductive spots with a small amount of film in contact with each other [3]. Electrical contacts cannot be separated, as the adhesion of the molten bridge makes it so the circuit is unable to work correctly after the molten bridge cools, which can cause a serious accident. Therefore, the arc erosion and welding resistance of electrical contacts need to be studied in a focused manner [4–9].

Copper (Cu) is widely used in electrical circuits due to its excellent electrical and thermal conductivity. However, the mechanical properties of pure copper are poor and need to be strengthened [10–12]. Therefore, developing copper matrix composites with excellent overall performance has become a hot research topic [13–16]. Dispersive copper matrix composites are used as a way to strengthen the copper matrix by introducing uniformly distributed nanoparticles with good thermal stability. The composites have high microstructure stability and are suitable for electrical contact field with high calorific value [17]. Among them, the aluminum oxide (Al_2O_3) dispersive copper matrix composites are more widely used to obtain diffuse fine Al_2O_3 nanoparticles, generally by internal oxidation of aluminum (Al) in Cu-Al alloy powders by cuprous oxide (Cu_2O) to improve the overall performance of the composites. Tian et al. [18] prepared Cu-0.5 vol.%Al_2O_3 composites with an electrical conductivity of 93% IACS and an ultimate tensile strength of 172 MPa at 600 °C. They concluded that the strengthening effect of alumina nanoparticles is not Orovan strengthening, but nanoparticle pegging at grain and subgrain boundaries, which hinders recrystallization. Zhang et al. [19] prepared Al_2O_3-Cu/(25)W(5)Cr and Al_2O_3-Cu/(35)W(5)Cr composites and found that the enhancement of W content could reduce the fusion welding force and improve the performance of the composites during electrical contact.

Adding high melting point hard phases such as molybdenum (Mo) and chromium (Cr) to the copper matrix helps improve the high-temperature performance of copper alloys or copper matrix composites. In addition, components with low melting points in the electrical contacts tend to melt into droplets and spatter out of the electrical contact surface due to Joule heating during electrical contact. On the contrary, the high melting point components can exist stably and form a skeleton-like structure to inhibit the spattering of low melting point components during electrical contact, maintaining a more stable contact interface [20,21]. Liang et al. [22] prepared Cu-5 wt.% Mo alloys by combining mechanical alloying with discharge plasma sintering and subjected them to rolling and aging treatment. The conductivity after rolling was 92.6% IACS and the microhardness reached 128.6 HV, and the conductivity of the alloy after aging reached 96.5% IACS with an anti-softening temperature of 950 °C. Chen et al. [23] prepared Mo-25Cu nanopowders by chemical co-deposition and hydrogen reduction, and the Vickers hardness of the pressed billets reached 2.68 GPa and the conductivity was 36.2% IACS. Şap et al. [24] prepared copper matrix composites with different Mo-SiCp powder additions using a powder metallurgical method. They investigated the effects of different sintering temperatures and sintering times on the properties of the composites. When the composites with Mo-SiCp addition of 5 wt.% were sintered at 1050 °C for 1 h, the composites had optimal densities, with an increase in the additional amount to 15 wt.%. The hardness of the composites could reach 77.038 HRB. Tantalum (Ta) has high hardness, melting point and toughness and good electrical and thermal conductivity and chemical stability. Copper-tantalum (Cu-Ta) alloys and copper-tantalum composites have far better mechanical and high-temperature properties than Cu [25–28]. For its excellent mechanical properties, the strengthening mechanism of Cu-Ta alloys has been recently investigated using molecular dynamics [29,30]. Li et al. [31] prepared Cu-Ta-Cr alloys using mechanical alloying and discharge plasma sintering techniques. They found that adding Cr significantly improved the dislocation pegging effect, thereby increasing Cu-Ta alloys' thermal stability and tensile strength. Wang et al. [32] performed kinetic simulations of Cu/Ta and Ta/Cu nanoindentation. They found that the Cu/Ta interface exhibited a solid barrier to dislocations crossing the interface, while the Ta/Cu interface could transfer deformation stress to activate Cu layer deformation. Hornbuckle et al. [33] investigated the growth rate of Cu-Ta alloys at high temperatures. They found that Cu-3 at.%Ta has outstanding high-temperature mechanical stability and extreme kinetics to withstand prolonged high-temperature exposure environments, which fits well with the need for electrical contacts to maintain stability under high-temperature operating conditions.

Nanoparticle-reinforced copper matrix composites are a promising direction for research, and widely used nanoparticles include tungsten carbide (WC) [34], silicon carbide (SiC), Al_2O_3, and yttria (Y_2O_3). Feng et al. [35] added SiC whiskers to Al_2O_3-Cu composites using powder metallurgy and hot extrusion. They found that the addition of SiC increased the yield strength and elongation of the composites by 6% and 15.6%, respectively. Pan et al. [36] prepared copper matrix composites with synergistic reinforcement of Al_2O_3 and carbon nanotubes using discharge plasma sintering. They found that nano-Al_2O_3 could disperse carbon nanotubes and inhibit grain growth, forming robust bonding interfaces. It was found that nano-Al_2O_3 could disperse carbon nanotubes and inhibit grain growth, forming robust bonding interfaces. The composites exhibited excellent mechanical properties and electrical conductivity of 345 MPa and 87.2% IACS, respectively. Li et al. [37] prepared W-Ni-Cu-Y_2O_3 alloy by cold pressing/sintering and found that Y_2O_3 could play a role in refining W grains. In addition, the addition of Y_2O_3 can enhance the density and microhardness of W-Ni-Cu alloy, and the dispersed Y_2O_3 can improve the mechanical properties of the alloy. Mu et al. [38] investigated the effect of Y_2O_3 addition on copper during electrical contact. They found that adding a small amount of Y_2O_3 can improve the hardness and density of the sample and reduce the material's electrical conductivity. The samples with Y_2O_3 addition maintained low contact resistance values after 20,000 arc ablation tests. Zhuo et al. [39] prepared Cu-Y_2O_3 composites with a strength of 568 MPa by liquid-phase in situ method and found a specific co-lattice relationship between Y_2O_3 and the copper matrix.

In this study, two high melting point phases, Mo and Ta, were added to the matrix based on Al_2O_3-Cu using a powder metallurgical method with a ball milling and fast hot pressing sintering technique to enhance the high-temperature stability and mechanical properties of the composites. In addition, a small amount of Y_2O_3 nanoparticles were added to improve the composites' electrical contact properties. The hardness, electrical conductivity and tensile strength of the sintered composites were measured, and the composites were characterized in terms of microstructure and electrical contact behavior using scanning electron microscopy, transmission electron microscopy and an electrical contact material testing system.

2. Materials and Methods

The metal powders used in this experiment are as follows: copper-aluminum (Cu-0.2 wt.%Al) alloy powders (purity > 99.9%, particle size < 38 μm), cuprous oxide powders (purity > 99.95%, particle size 2 μm–5 μm), molybdenum powders (purity > 99.95%, particle size 5 μm–8 μm), tantalum powders (purity > 99.95%, particle size 3 μm–8 μm) and yttrium oxide powders (purity > 99.99%, particle size < 5 nm). The metal powders and cuprous oxide powders were purchased from Shanghai Bowei Technology Co. (Shanghai, China). The yttrium oxide powders were purchased from Shanghai Aladdin Biochemical Technology Co., Ltd. (Shanghai, China). The initial powder morphology is shown in Figure 1a–e. The copper-aluminum (Cu-0.2 wt.%Al) alloy powders, Mo powders, Ta powders, Cu_2O powders and Y_2O_3 powders were weighed according to the composition ratio shown in Table 1, and the weighed components were added to the mixing tank in turn. The mixing tank was placed on the QQM/B tank mill at 50 rpm for 8 h to obtain Cu-0.2Al-Cu_2O-25Mo-5Ta and 0.5Y_2O_3-Cu-0.2Al-Cu_2O-25Mo-5Ta composite powders, as shown in Figure 1f–i. After 8 h of ball milling mixing, the composite powders in the mixing tank were transferred to a cylindrical graphite mold of Φ30 mm and pre-pressed by a small hydraulic press. The pre-pressed molds were placed in the FHP-828 fast hot-pressing sintering furnace for fast hot-pressing sintering. The furnace cavity is first vacuumed to below 10^{-2} Pa, then heated to 750 °C at a heating rate of 100 °C/min and an axial pressure of 30 MPa, where the mold is held for 2 min. At the end of the holding process, the mold is cooled to room temperature and then demolded to obtain the corresponding composite sintered specimens.
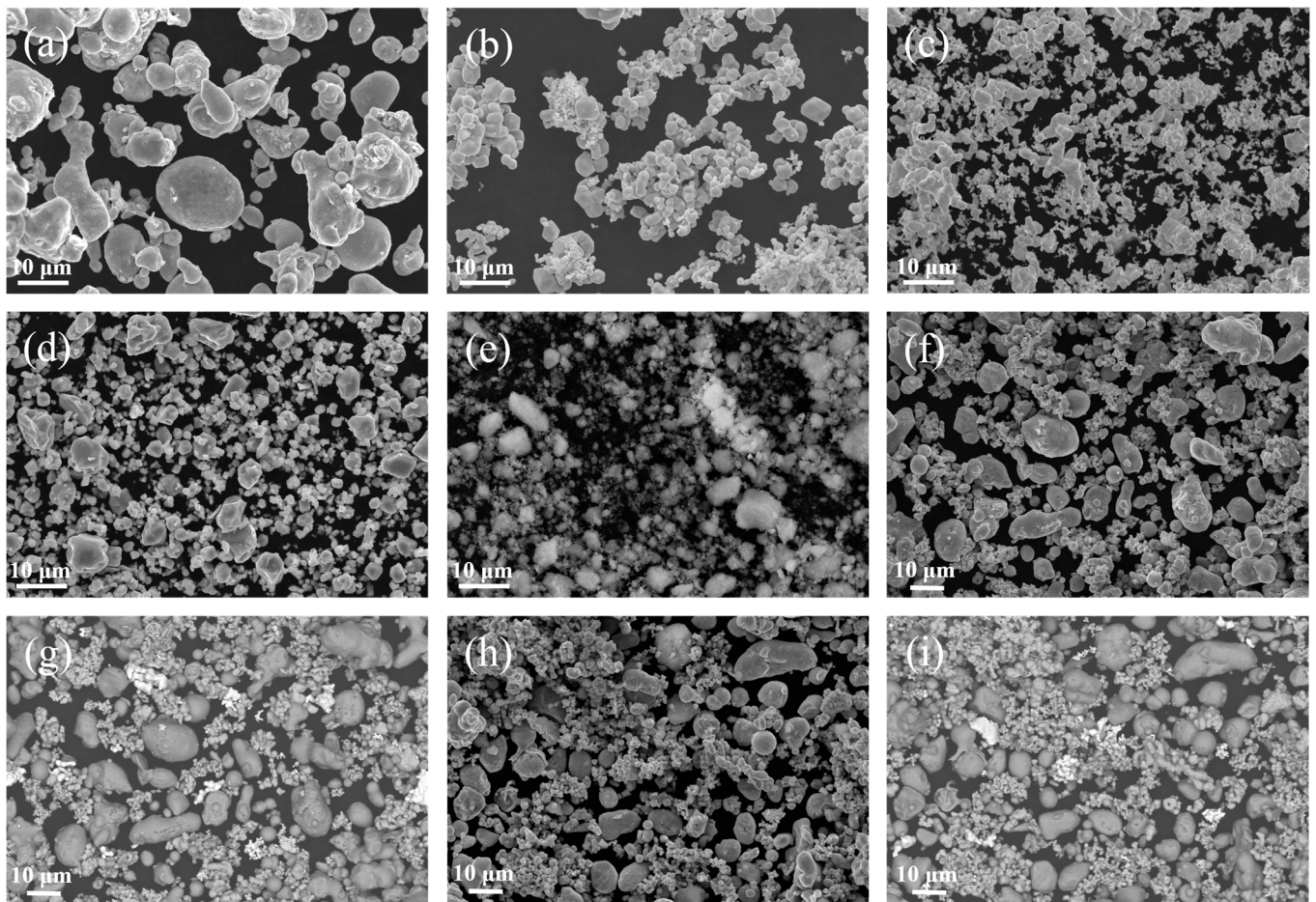
Figure 1. SEM of initial powders and composite powders: (**a**) Cu-0.2 wt.%Al powders; (**b**) Mo powders; (**c**) Ta powders; (**d**) Cu_2O powders; (**e**) Y_2O_3 powders; (**f**) Cu-0.2Al-Cu_2O-25Mo-5Ta mixed powders after ball milling; (**g**) Cu-0.2Al-Cu_2O-25Mo-5Ta mixed powders after ball milling in backscattering mode; (**h**) 0.5Y_2O_3-Cu-0.2Al-Cu_2O-25Mo-5Ta mixed powders after ball milling; (**i**) 0.5Y_2O_3-Cu-0.2Al-Cu_2O-25Mo-5Ta mixed powders after ball milling in backscattering mode.

Table 1. Theoretical compositions of the composites (wt.%).

Composites	Cu-0.2 wt.%Al	Cu_2O	Mo	Ta	Y_2O_3
Al_2O_3-Cu/25Mo5Ta	bal.	2.04	25	5	0
0.5Y_2O_3/Al_2O_3-Cu/25Mo5Ta	bal.	2.02	25	5	0.5

The sintered specimens were sanded and polished using sandpaper (400#, 800#, 1200#, 1500#, 2000#) and a polisher and then tested for performance. The electrical conductivity of the sintered specimens was measured using a Sigma 2008-B eddy current tester (Xiamen Tianyan Instrument Co. Ltd., Xiamen, China). The Vickers hardness of the sintered specimens was measured using an HV-100 Vickers hardness tester. The dry and wet weights of the sintered specimens were measured using an MS304S hydrostatic balance (the specimens were immersed in deionized water for 24 h). The densities were determined using the Archimedes drainage method. The results of the above performance tests were averaged over five sets of test data. The composite materials were processed into dog-bone specimens using a wire cutter and tested by a Shimadzu AG-I 250 kN universal testing machine (Shimadzu Co., Kyoto, Japan) at a rate of 1 mm/min for room-temperature tensile testing. Table 2 shows the comprehensive performance of the two composites.

**Table 2.** Comprehensive performance of composite materials.

Composites	Hardness (HV)	Electrical Conductivity (% IACS)	Relative Density (%)	Tensile Strength (MPa)	Elongation (%)
Al_2O_3-Cu/25Mo5Ta	164	68.92	98.52	333	8.74
$0.5Y_2O_3/Al_2O_3$-Cu/25Mo5Ta	156	67.54	97.75	325	9.46

The sintered specimens were processed into electrical contact specimens of $\Phi 3.8$ mm $\times$ 10 mm using a wire cutter, and the surface oxide was removed by sandpaper. The JF04C electrical contact test system (Kunming Guiyan Jinfeng Technology Co. Ltd., Kunming, China) was used to test the processed electrical contact specimens with a voltage of DC 30 V, 10 A–30 A and a contact closure frequency of 1 Hz for 10,000 contact closures. The cathode contacts were weighed before and after the electrical contact test using a BSM-120.4 electronic balance to characterize the mass transfer of the electrical contacts before and after the electrical contact process. A JSM-IT100 scanning electron microscope (JEOL Ltd., Tokyo, Japan) was used to observe the microscopic morphology of the composite materials after the electrical contact test. The sintered state specimens of the composites were characterized using a field emission transmission electron microscope (FEI Tecnai F30, Thermo Fisher Scientific Inc., Waltham, MA, USA).

3. Results

### 3.1. Electrical Contact Performance

Figure 2 shows the mass transfer of the cathode and anode of two electrical contact materials at different currents before and after electrical contact. The value of the cathode and anode is the mass after the electrical contact test minus the mass before the electrical contact test. The overall value is the anode's mass minus the cathode's mass. A positive value for the total mass transfer represents the mass transfer from the electrical contact to the cathode and vice versa for the cathode to the anode. From Figure 2a,b, it can be seen that the change in the cathode to anode mass of both electrical contacts increases as the current increases, which indicates that more material transfer occurs during the electrical contact. This is because the contact area is constant and the contact resistance does not fluctuate much under controlled closure pressure. The higher the current, the greater the Joule heat generated during the electrical contact. The Cu with a low melting point forms more molten bridges or droplets after melting, which move between the electrical contacts with the movement of the electrical contacts. When the Joule heat released during the electrical contact is too large, the melted Cu droplets will be sprayed outside the electrical contact surface due to the movement of the electrical contact, resulting in the loss of electrical contact mass. However, the mass loss of both electrical contact materials during the electrical contact was small relative to the cathode mass, which indicates that the melted Cu droplets were well controlled on the electrical contact surface. Comparing Figure 2a,b, it can be seen that the addition of Y_2O_3 reduces the mass change in both cathode and anode electrical contacts, which indicates that Y_2O_3 can suppress the spattering of Cu droplets and has a positive effect on the stability and lifetime of the electrical contacts.
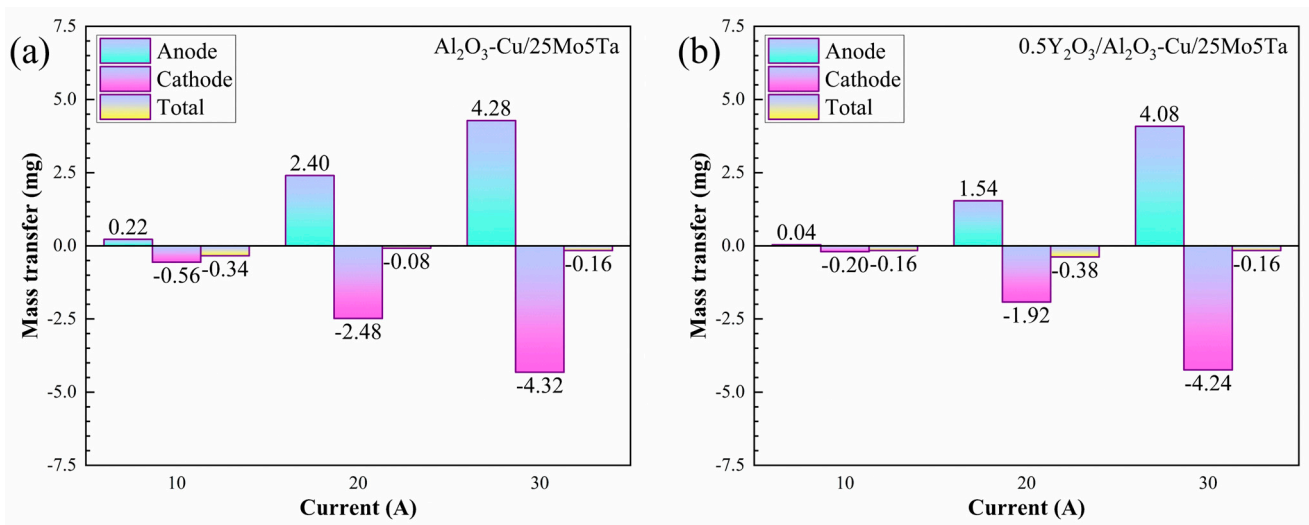
Figure 2. Mass transfer for electrical contacts in different current: (**a**) Al_2O_3-Cu/25Mo5Ta composites; (**b**) $0.5Y_2O_3/Al_2O_3$-Cu/25Mo5Ta composites.

In order to further investigate the mass transfer mechanism of Al_2O_3-Cu/25Mo5Ta and $0.5Y_2O_3/Al_2O_3$-Cu/25Mo5Ta electrical contact materials during electrical contact, the electrical contacts were characterized by SEM. Figure 3 shows the SEM images of the cathode electrical contacts after the electrical contact test. Figure 3a–c show the Al_2O_3-Cu/25Mo5Ta and $0.5Y_2O_3/Al_2O_3$-Cu/25Mo5Ta electrical contact materials at different currents. The surface of all three electrical contact materials showed craters of different sizes. This is due to the fatigue and loosening of the grains on the contact surface when the electrical contacts were repeatedly closed several times, followed by the accumulation of air absorption when the electrical contacts were disconnected. When the contacts are closed afterward, the protrusions will hit the corresponding position of the other contact and form craters, and the grains near the craters will continue to produce protrusions by extrusion. The cathode and anode contacts repeatedly interact with each other to form large-sized, uniformly dispersed craters. As the current increases, the arc erosion phenomenon becomes more evident, as can be seen by comparing Figure 3a–c. This is because the contact between the electrical contacts is a point contact rather than a surface contact. When the electrical contacts are heated and melted, the cooled metal droplets solidify on the surface of the electrical contacts. As the number of contacts increases, the heat accumulated cannot be exported from the base in time and the electrical contact temperature rises together, leading to high contact surface temperatures, causing contact surface softening and increasing the contact area when the contact is closed. As a result, the area where arc erosion occurs is more extensive. The area of arc erosion reduced after adding Y_2O_3, which indicates that Y_2O_3 can enhance the arc erosion resistance of electrical contact materials to some extent. Figure 3d shows the anode morphology of Al_2O_3-Cu/25Mo5Ta electric contact material at 30 A. It can be seen that there are solidified droplets. Figure 3e shows the cathode morphology of the Al_2O_3-Cu/25Mo5Ta electrical contact material at 30 A. The metal skeleton can be observed. The solidified droplets are present inside the metal skeleton. It can be speculated that the Cu splash out of the electrical contact surface forms a skeleton of Mo or Ta after melting by heat, as Mo and Ta remain stable at high temperatures. Moreover, the capillary effect of the skeleton will inhibit the spattering of Cu droplets, reducing the material transfer during the operation of the electric contact and improving the electric contact's performance and life. Figure 3f shows the anode morphology of the $0.5Y_2O_3/Al_2O_3$-Cu/25Mo5Ta electrical contact material at 30 A. It can be seen that the surface droplets are more finely dispersed and there are small and dense holes compared with the electric contact material without Y_2O_3 addition. Figure 3g–i show the $0.5Y_2O_3/Al_2O_3$-Cu/25Mo5Ta electrical contact material at a magnification of 30 A. Protrusions with a horizontal cross-sectional diameter of about 10 µm–20 µm at the

bottom can be observed. These protrusions generate a large amount of Joule heat during the electrical contact due to the contraction of the arc line, which causes the surrounding Cu to melt and splash so that many holes exist below the protrusions, and the surrounding area is a concentration of liquid droplets. In addition, the formation of the protrusions leads to an increase in the contact pressure and the formation of microcracks in their vicinity due to uneven stresses, typical of arc erosion morphology. Zhang et al. [19] carried out 10,000 electrical contact opening and closing tests on the Al_2O_3-Cu/(25)W(5)Cr composites at DC 30 V, 30 A, and characterized the ablation morphology of the composites. It can be seen that the Al_2O_3-Cu/25Mo5Ta composites show more excellent arc erosion resistance in 10,000 electric contact opening and closing tests, which is reflected in the smaller area of the arc erosion morphology and the smoother morphology after the arc erosion. This is because the high temperature resistance of Mo and Ta is better than that of Cr, and the electric contacts are more stable in a long-term high-temperature environment.
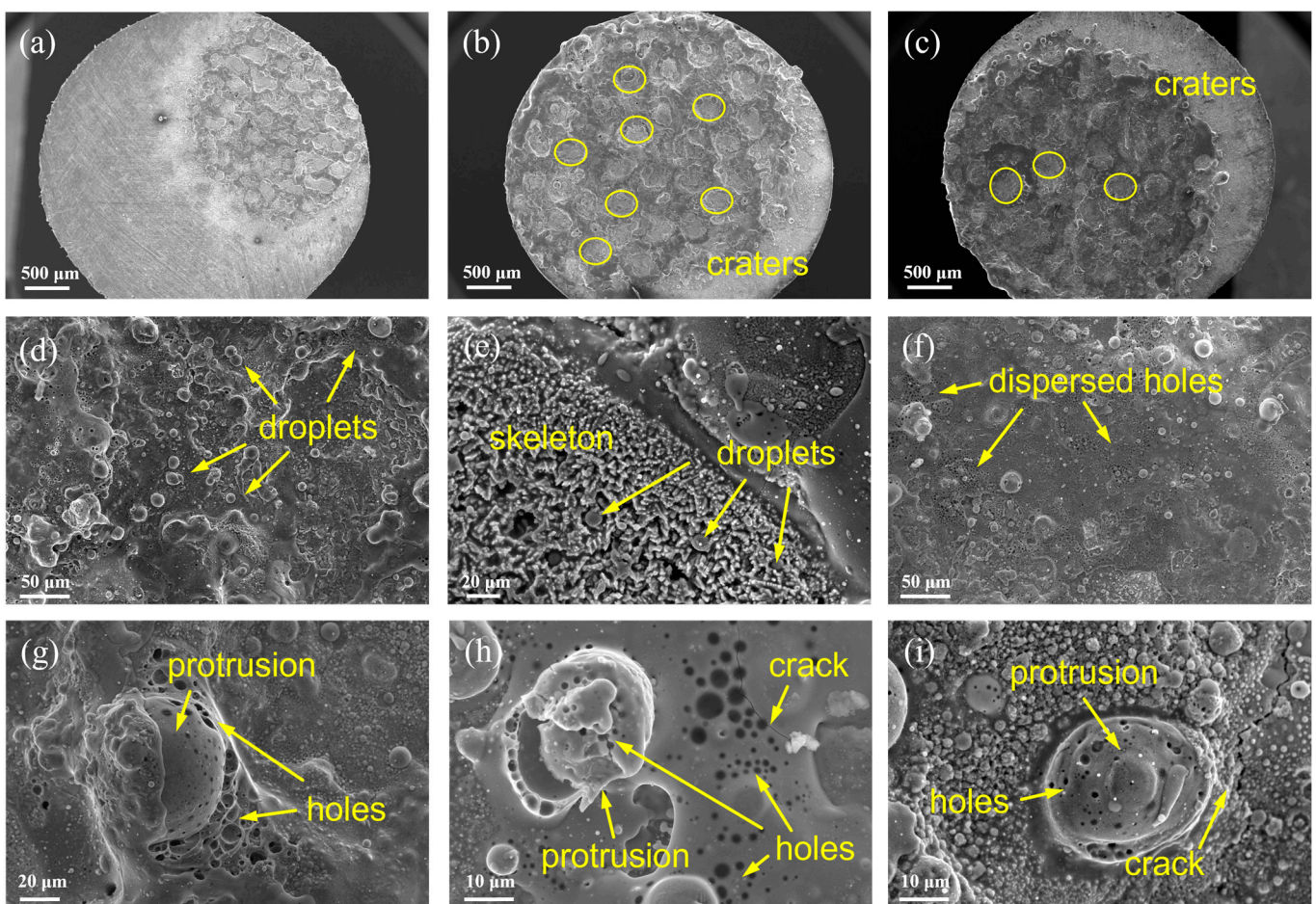
Figure 3. SEM images of electric contact materials after arc erosion: (**a**) Al_2O_3-Cu/25Mo5Ta anode at 10 A; (**b**) Al_2O_3-Cu/25Mo5Ta anode at 30 A; (**c**) $0.5Y_2O_3/Al_2O_3$-Cu/25Mo5Ta anode at 30 A; (**d**) Al_2O_3-Cu/25Mo5Ta anode at 10 A; (**e**) Al_2O_3-Cu/25Mo5Ta cathode at 10 A; (**f**) Al_2O_3-Cu/25Mo5Ta anode at 30 A; (**g–i**) $0.5Y_2O_3/Al_2O_3$-Cu/25Mo5Ta cathode at 30 A.

During the electrical contact, an arc can be generated between the cathode and anode during the opening and closing process under voltage. Since the electrical contact surface is not perfectly flat, the arc will be concentrated in the protrusion of the electrical contact surface. The high electric field strength generated during the closing process causes the electrical contact surface to arc and release much Joule heat. If the arc intensity is too high, the risk of fusion welding of electrical contacts increases. In order to investigate the behavior of the electrical contact material during circuit opening and closing, the arc

duration and arc energy were analyzed. The data collected at every 100 disconnection closures were averaged and the results are shown in Figure 4. Figure 4a–f show the variation in the arc duration and arc energy with the number of electrical contact closures for Al_2O_3-Cu/25Mo5Ta and $0.5Y_2O_3/Al_2O_3$-Cu/25Mo5Ta electrical contact materials at DC 30 V, 10 A–30 A, respectively. Both composites' arc duration and arc energy first showed low levels at 10 A current. As the number of contacts increased, both showed a sudden increase, followed by a slight decrease. This is because when the current is small, the electric field strength generated when the contacts are closed is relatively small, the energy to maintain the arc is low, and the generated arc is small. When the number of electrical contacts reaches about 1600, the arc duration and arc energy rise sharply. This may be due to the typical arc erosion morphology due to the erosion of the electrical contacts as the number of electrical contacts rises. The increase in protrusion leads to an increase in arc duration, which causes an increase in energy. A similar pattern can be observed when the current increases to 20 A compared to 30 A. The arc duration increases with the number of contacts and then maintains a relatively stable level. It is worth noting that as the current increases, the number of electrical contacts required to improve the arc duration time gradually decreases. This is because the higher the current, the more severe the arc erosion phenomenon and the faster the relative stability is reached. It can be seen that both the arc duration time and the arc energy of the $0.5Y_2O_3/Al_2O_3$-Cu/25Mo5Ta electrical contact material are elevated more slowly compared to the Al_2O_3-Cu/25Mo5Ta electrical contact material. This is a good indication that the addition of Y_2O_3 effectively suppresses the arc-burning phenomenon during electrical contact, which positively impacts the life and safety of electrical contacts.
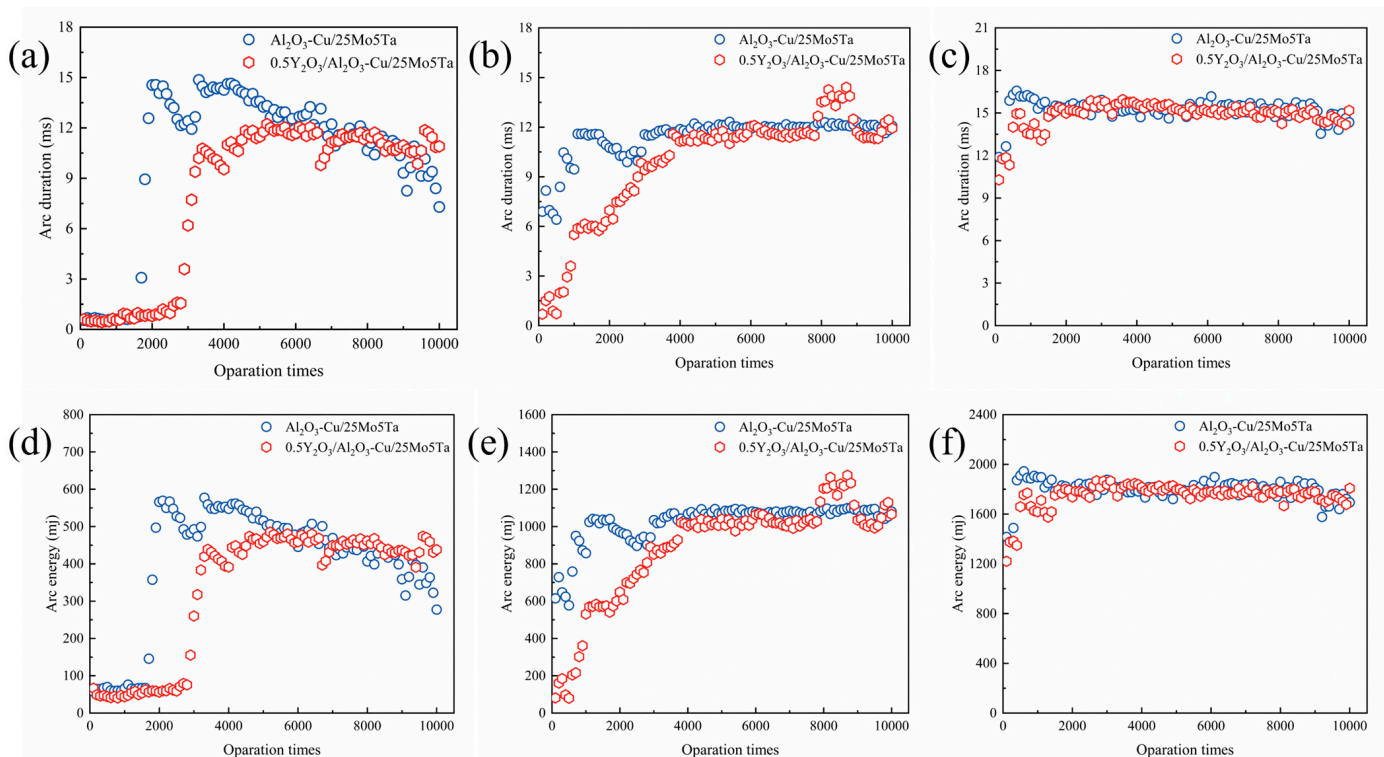
Figure 4. Variation of arc duration and arc energy with the operation times for Al_2O_3-Cu/25Mo5Ta and $0.5Y_2O_3/Al_2O_3$-Cu/25Mo5Ta electrical contact materials: (**a**) 10 A; (**b**) 20 A; (**c**) 30 A; (**d**) 10 A; (**e**) 20 A; (**f**) 30 A.

The metal is subjected to high temperatures and local melting occurs. The molten bridge will stick to the static and dynamic contacts after cooling, leading to melting welding when the electrical contacts are closed. Two measures can be taken to prevent the occurrence of melt welding, respectively, to improve the segmentation force and the material

resistance to melt welding properties. In this work, the closure pressure was controlled to be 40 cN–60 cN to reduce the effect of the segmentation force on the fusion welding force. Figure 5 shows the trend of melt welding force with the number of operations for two composites at different currents, averaged over every 100 sets of data. As the current increases, the welding force of the composites increases slightly. This is because the higher current generates more Joule heat, which causes the electrical contacts to melt, resulting in a higher melt welding tendency. There is a slight decrease in the welding force of the composite after the addition of Y_2O_3 and it shows a hysteresis. As the number of contacts increased, the welding force of the composites showed a segmented up-steep-down-up trend. During the contacting process, the mass transfer from cathode to anode occurs continuously during the formation and disconnection of the fusion bridge, and the protrusion on the surface of the electrical contact increases gradually, leading to the enrichment of Cu liquid. After the mass transfer of the electrical contact reaches a certain level, the next contact will significantly change the shape of the electrical contact surface. After the molten bridge melts, a large amount of Cu liquid is drawn in by the capillary action of the cathodic Mo skeleton and the height of the protrusions re-form when the electrical contact that is disconnected decreases, leading to a reduction in fusion welding force. This is confirmed by the hysteresis exhibited by the addition of Y_2O_3, which increases the high-temperature stability of the composite and reduces the rate of Cu liquid enrichment, pushing back the time of the steep drop. The steep drop in weld force is more pronounced at low currents, while it is more hysteretic at high currents. This is due to the small mass transfer per contact at low currents, the slow growth rate of the protrusion, and the higher number of times required to break the protrusion. Under the high current, the mass transfer is fast and the heat generation is high and the protrusions complete the accumulation and destruction cycles more frequently, so the increase is less pronounced and the steep drop is less likely to occur.
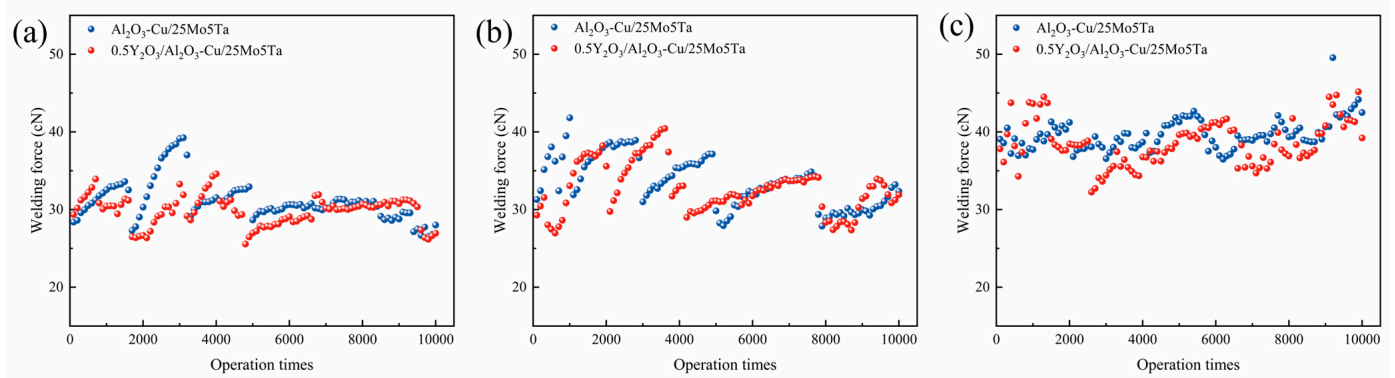
Figure 5. Variation of welding force with the operation times for Al_2O_3-Cu/25Mo5Ta and $0.5Y_2O_3/Al_2O_3$-Cu/25Mo5Ta electrical contact materials: (**a**) 10 A; (**b**) 20 A; (**c**) 30 A.

In order to explore the overall impact of Y_2O_3 addition on the electrical contact performance of electrical contact materials, the average value of 10,000 circuit opening and closing tests for a single round was calculated, including the arc duration, arc energy and welding force. The results are shown in Figure 6. It can be seen that all three sets of data increase as the current increases. Adding Y_2O_3 reduces the average arc duration and average arc energy in the same voltage and current conditions. The arc suppression effect of Y_2O_3 is more prominent under a lower current. Combined with the erosion morphology of electrical contacts in Figure 3 and the variation in arc duration and arc energy with the number of contacts shown in Figure 4, it can be assumed that the erosion of the electrical contact surface becomes more severe with the increase in current. Copper with a low melting point was gradually enriched, resulting in a decrease in the contact surface Y_2O_3 percentage content and the inhibitory effect on the arc was gradually weakened. After adding Y_2O_3, the average arc duration of 10 A–30 A decreased by 21.53%, 13.77% and 2.24%, and the average arc energy decreased by 18.02%, 13.56% and 2.42%, respectively. Figure 6c

shows that the addition of Y_2O_3 reduces the fusion welding force of the composites. This demonstrates that adding Y_2O_3 can effectively improve the electrical contact properties of the composites from two aspects of arc extinguishing and welding resistance. Liu et al. [40] studied the welding force of $Cu/0.5CeO_230Cr$ composites during DC 25V, 30A electric contact. It can be seen that the Al_2O_3-Cu/25Mo5Ta composites exhibit a smaller welding force under the same current and higher voltage. This is because the high-temperature stability of dispersion strengthened copper matrix is better than that of pure copper and the high-temperature stability of the second phase is also higher than that of Cr. When a large amount of heat passes through the electric contact, the Al_2O_3-Cu/25Mo5Ta composite is more difficult to soften.
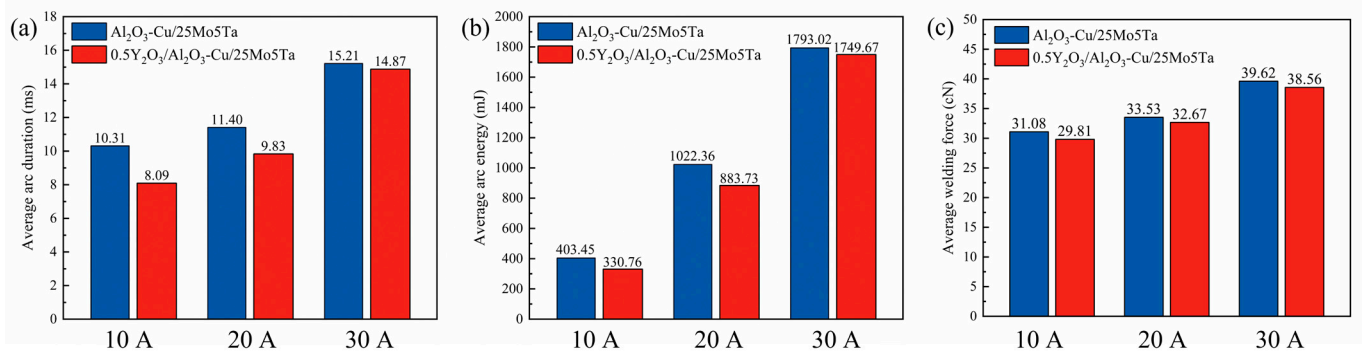
Figure 6. Electrical contact properties of Al_2O_3-Cu/25Mo5Ta and $0.5Y_2O_3/Al_2O_3$-Cu/25Mo5Ta electrical contact materials: (**a**) Average arc duration; (**b**) Average arc energy; (**c**) Average welding force.

3.2. Microstructural Characterization

To reveal the effect of Y_2O_3 on the electrical contact behavior, the $0.5Y_2O_3/Al_2O_3$-Cu/25Mo5Ta electrical contact material was characterized using TEM, as shown in Figure 7. Figure 7a–c shows the bright-field TEM images of $0.5Y_2O_3/Al_2O_3$-Cu/25Mo5Ta composites. As seen in Figure 7a, the nanoparticles are uniformly and diffusely distributed in the matrix. Previous studies have shown that this nanoparticle is γ-Al_2O_3, which acts as a diffuse reinforcement to the matrix [19]. From Figure 7b, it can be seen that Al_2O_3 is present in the matrix in another form. Compared to γ-Al_2O_3, this Al_2O_3 is more prominent in size and appears in grain or phase boundaries, acting as a pinned grain boundary. A study by Pethő et al. [41] showed that α-Al_2O_3 in Cu-Mo composites prepared by hot-press sintering would only aggregate on Mo grain boundaries, which is consistent with the observed phenomenon. A more complex phase distribution is observed in Figure 7c, where the region in the yellow square is presented as a dark field phase, as shown in Figure 7d. As shown in Figure 7d, EDS analysis was performed in Figure 7e. It can be seen from the EDS image that there are Al oxides and Y oxides of larger sizes in the composite. Figure 7f shows the selected electron diffraction spot of region 1 of Figure 7d, and it is known that $YTaO_4$ and Ta monomers are present in this region after calibration. The HRTEM characterization at the two-phase interface in the region of Figure 7d results in monoclinic $YTaO_4$ on the left side, as shown in Figure 7g. Zhou et al. [42] analyzed $YTaO_4$ with three different structures based on the firstness principle and concluded that the monoclinic phase has the highest Young's modulus. Zhang et al. [43] also concluded that the monoclinic $YTaO_4$ is a thermodynamically stable phase based on the firstness principle. In addition, $YTaO_4$ has been applied in thermal barrier coating materials due to its excellent thermal stability [44–46]. The geometric phase analysis (GPA) of Figure 7g was performed as shown in Figure 7h. It can be seen from the figure that the part corresponding to $YTaO_4$ shows red and green color, i.e., it is subjected to less strain, and the right matrix part shows yellow and blue color, i.e., it is subjected to more strain. It can be reasonably speculated that $YTaO_4$ has a positive effect on the mechanical properties of the composites.
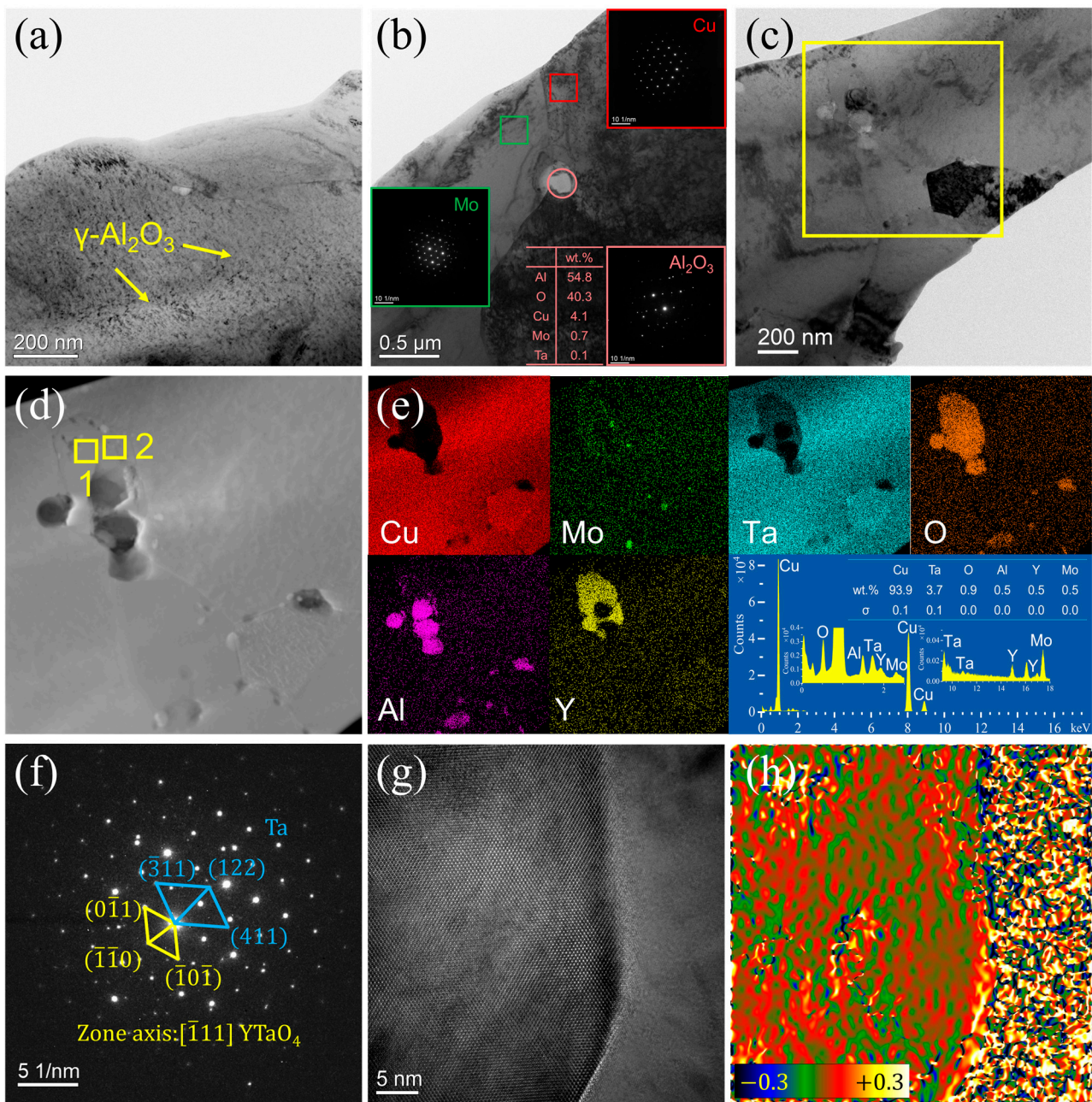
Figure 7. TEM images of $0.5Y_2O_3/Al_2O_3\text{-}Cu/25Mo5Ta$ composites: (**a–c**) Bright-field TEM images of composites; (**d**) Dark-field phase of (**c**); (**e**) EDS images of (**d**); (**f**) SADP of region 1 in (**d**); (**g**) HRTEM images of region 2 in (**d**); (**h**) GPA of (**g**).

4. Conclusions

$Al_2O_3\text{-}Cu/25Mo5Ta$ and $0.5Y_2O_3/Al_2O_3\text{-}Cu/25Mo5Ta$ composites were prepared using powder metallurgy and fast hot-pressing sintering. The physical and electrical contact properties of the composites were investigated. The microstructure of the composites was characterized with TEM. The main conclusions were derived as follows:

(1) The electrical contact mass transfer direction of $Al_2O_3\text{-}Cu/25Mo5Ta$ and $0.5\ Y_2O_3/Al_2O_3\text{-}Cu/25Mo5Ta$ composites is from cathode to anode, and the addition of Y_2O_3 can reduce the mass loss of electrical contacts.

(2) Y_2O_3 can slow down the erosion rate of $Al_2O_3\text{-}Cu/25Mo5Ta$ electrical contact composites and the growth rate of arc duration and arc energy. In addition, Y_2O_3 can reduce the average arc duration and average arc energy of $Al_2O_3\text{-}Cu/25Mo5Ta$. At 10 A current, the average arc duration and average arc energy decreased to 21.53% and 18.02%, respectively.

Therefore, Y_2O_3 positively affects the arc erosion resistance of Al_2O_3-Cu/25Mo5Ta electrical contact composites.

(3) Y_2O_3 can improve the anti-welding performance of composites, which is manifested by the decrease in welding force and the hysteresis of the change in welding force.

(4) The nanoscale $YTaO_4$ formed during the sintering process of $0.5Y_2O_3/Al_2O_3$-Cu/25Mo5Ta composites. The high thermomechanical stability and excellent mechanical properties of $YTaO_4$ positively influence the composites' high-temperature stability and mechanical properties.

(5) The conductivity of the $0.5Y_2O_3/Al_2O_3$-Cu/25Mo5Ta composites was 67.54% IACS and the tensile strength was 325 MPa. The addition of Y_2O_3 had almost no negative effect on the conductivity and tensile strength of the composites.

Author Contributions: Conceptualization, Y.L. (Yunzhang Li) and B.T.; methodology, Y.L. (Yunzhang Li); formal analysis, Y.L. (Yunzhang Li), H.Z., X.Z., S.L. and C.Z.; investigation, Y.L. (Yunzhang Li), S.T. and X.L.; resources, M.Z., B.T. and Y.L. (Yong Liu); writing—original draft preparation, Y.L. (Yunzhang Li); writing—review and editing, Y.Z. and A.A.V.; supervision, M.Z., Y.Z., B.T. and Y.L. (Yong Liu); project administration, M.Z.; funding acquisition, M.Z. and Y.Z. All authors have read and agreed to the published version of the manuscript.

Institutional Review Board Statement: Not applicable.

Informed Consent Statement: Not applicable.

Data Availability Statement: All data that support the findings of this study are included within the article.

Conflicts of Interest: The authors declare no conflict of interest.

References

1. Cui, R.; Han, Y.; Zhu, Z.; Chen, B.; Ding, Y.; Zhang, Q.; Wang, Q.; Ma, G.; Pei, F.; Ye, Z. Investigation of the Structure and Properties of Electrodeposited Cu/Graphene Composite Coatings for the Electrical Contact Materials of an Ultrahigh Voltage Circuit Breaker. *J. Alloys Compd.* **2019**, *777*, 1159–1167. [CrossRef]
2. Bodrova, L.E.; Melchakov, S.Y.; Shubin, A.B.; Goyda, E.Y. Smart-Microstructures of Composites for Electrical Contacts with Frameless Packing of Cr and W in Copper. *Trans. Nonferrous Met. Soc. China* **2021**, *31*, 2773–2786. [CrossRef]
3. Razi-Kazemi, A.A.; Abdollah, M. Novel High-Frequency-Based Diagnostic Approach for Main Contact Assessment of High-Voltage Circuit Breakers. *IET Gener. Transm. Distrib.* **2018**, *12*, 1121–1126. [CrossRef]
4. Huang, R.; Xu, G.; Wu, Q.; Yuan, M.; Wu, C. Influence of Operation Number on Arc Erosion Behavior of Ag/Ni Electrical Contact Materials. *Trans. Nonferrous Met. Soc. China* **2022**, *32*, 2681–2695. [CrossRef]
5. Li, W.-J.; Chen, Z.-Y.; Jiang, H.; Sui, X.-H.; Zhao, C.-F.; Zhen, L.; Shao, W.-Z. Effects of Interfacial Wettability on Arc Erosion Behavior of Zn_2SnO_4/Cu Electrical Contacts. *J. Mater. Sci. Technol.* **2022**, *109*, 64–75. [CrossRef]
6. Lin, Z.; Fan, S.; Liu, M.; Liu, S.; Li, J.-G.; Li, J.; Xie, M.; Chen, J.; Sun, X. Excellent Anti-Arc Erosion Performance and Corresponding Mechanisms of a Nickel-Belt-Reinforced Silver-Based Electrical Contact Material. *J. Alloys Compd.* **2019**, *788*, 163–171. [CrossRef]
7. Kesim, M.T.; Yu, H.; Sun, Y.; Aindow, M.; Alpay, S.P. Corrosion, Oxidation, Erosion and Performance of Ag/W-Based Circuit Breaker Contacts: A Review. *Corros. Sci.* **2018**, *135*, 12–34. [CrossRef]
8. Jeong, H.T.; Kim, W.J. Comparison of Hot Deformation Behavior Characteristics Between As-Cast and Extruded Al-Zn-Mg-Cu (7075) Aluminum Alloys with a Similar Grain Size. *Materials* **2019**, *12*, 3807. [CrossRef]
9. Wang, D.; Tian, W.; Lu, C.; Ding, J.; Zhu, Y.; Zhang, M.; Zhang, P.; Sun, Z. Comparison of the Interfacial Reactions and Properties between Ag/Ti_3AlC_2 and Ag/Ti_3SiC_2 Electrical Contact Materials. *J. Alloys Compd.* **2021**, *857*, 157588. [CrossRef]
10. Güler, Ö.; Bağcı, N. A Short Review on Mechanical Properties of Graphene Reinforced Metal Matrix Composites. *J. Mater. Res. Technol.* **2020**, *9*, 6808–6833. [CrossRef]
11. Zhou, M.; Geng, Y.; Zhang, Y.; Ban, Y.; Li, X.; Jia, Y.; Liang, S.; Tian, B.; Liu, Y.; Volinsky, A.A. Enhanced Mechanical Properties and High Electrical Conductivity of Copper Alloy via Dual-Nanoprecipitation. *Mater. Charact.* **2023**, *195*, 112494. [CrossRef]
12. Salvo, C.; Mangalaraja, R.V.; Udayabashkar, R.; Lopez, M.; Aguilar, C. Enhanced Mechanical and Electrical Properties of Novel Graphene Reinforced Copper Matrix Composites. *J. Alloys Compd.* **2019**, *777*, 309–316. [CrossRef]

13. Zhang, X.; Xu, Y.; Wang, M.; Liu, E.; Zhao, N.; Shi, C.; Lin, D.; Zhu, F.; He, C. A Powder-Metallurgy-Based Strategy toward Three-Dimensional Graphene-like Network for Reinforcing Copper Matrix Composites. *Nat. Commun.* **2020**, *11*, 2775. [CrossRef] [PubMed]

14. Cao, M.; Xiong, D.-B.; Yang, L.; Li, S.; Xie, Y.; Guo, Q.; Li, Z.; Adams, H.; Gu, J.; Fan, T.; et al. Ultrahigh Electrical Conductivity of Graphene Embedded in Metals. *Adv. Funct. Mater.* **2019**, *29*, 1806792. [CrossRef]

15. Liu, X.; Cai, Z.; xiao, Q.; Shen, M.; Yang, W.; Chen, D. Fretting Wear Behavior of Brass/Copper-Graphite Composites as a Contactor Material under Electrical Contact. *Int. J. Mech. Sci.* **2020**, *184*, 105703. [CrossRef]

16. Mousavi, Z.; Pourabdoli, M. Physical and Chemical Properties of Ag–Cu Composite Electrical Contacts Prepared by Cold-Press and Sintering of Silver-Coated Copper Powder. *Mater. Chem. Phys.* **2022**, *290*, 126608. [CrossRef]

17. Dong, L.; Li, L.; Li, X.; Zhang, W.; Fu, Y.; Elmarakbi, A.; Zhang, Y. Enhancing Mechanisms of Arc-Erosion Resistance for Copper Tungsten Electrical Contact Using Reduced Graphene Oxides in Situ Modified by Copper Nanoparticles. *Int. J. Refract. Met. Hard Mater.* **2022**, *108*, 105934. [CrossRef]

18. Tian, B.; Liu, P.; Song, K.; Li, Y.; Liu, Y.; Ren, F.; Su, J. Microstructure and Properties at Elevated Temperature of a Nano- Al_2O_3 Particles Dispersion-Strengthened Copper Base Composite. *Mater. Sci. Eng. A* **2006**, *435–436*, 705–710. [CrossRef]

19. Zhang, X.; Zhang, Y.; Tian, B.; An, J.; Zhao, Z.; Volinsky, A.A.; Liu, Y.; Song, K. Arc Erosion Behavior of the Al_2O_3-Cu/(W, Cr) Electrical Contacts. *Compos. Part B Eng.* **2019**, *160*, 110–118. [CrossRef]

20. Liang, S.; Li, Y.; Zhang, Y.; Zhou, M.; Liu, S.; Li, X.; Geng, Y.; Tian, B.; Jia, Y.; Liu, Y.; et al. Mechanical and Electrical Properties of $Cu_{30}Cr_{0.2}$Zr Composites Enhanced by CeO_2/GO. *J. Alloys Compd.* **2023**, *934*, 167759. [CrossRef]

21. Li, L.; Liu, S.; Zhou, M.; Zhang, Y.; Liang, S.; Huang, J.; Tian, B.; Geng, Y.; Ban, Y.; Liu, Y.; et al. Microstructure Evolution of Graphene Reinforced Cu/CeO_2/Cr Electrical Contact Materials under Thermal Deformation Behavior. *J. Mater. Res. Technol.* **2022**, *18*, 1412–1423. [CrossRef]

22. Liang, Y.; Lei, Q.; Zhang, X.; Jiang, D.; Li, Y. Microstructure Evolution and Properties of a Cu-5 Wt% Mo Alloy with High Conductivity and High Anti-Soften Temperature. *Mater. Today Commun.* **2022**, *32*, 104134. [CrossRef]

23. Chen, Q.; Liang, S.; Zhuo, L. Fabrication and Characterization of Mo-Cu Nano-Composite Powders by a Chemical Co-Deposition Technique. *J. Alloys Compd.* **2021**, *875*, 160026. [CrossRef]

24. Şap, E. Investigation of Mechanical Properties of Cu/Mo-SiCp Composites Produced with P/M, and Their Wear Behaviour with the Taguchi Method. *Ceram. Int.* **2021**, *47*, 25910–25920. [CrossRef]

25. Mousavi, T.; Dai, J.; Bazarnik, P.; Pereira, P.H.R.; Huang, Y.; Lewandowska, M.; Langdon, T.G. Fabrication and Characterization of Nanostructured Immiscible Cu–Ta Alloys Processed by High-Pressure Torsion. *J. Alloy. Compd.* **2020**, *832*, 155007. [CrossRef]

26. Zeng, L.F.; Gao, R.; Fang, Q.F.; Wang, X.P.; Xie, Z.M.; Miao, S.; Hao, T.; Zhang, T. High Strength and Thermal Stability of Bulk Cu/Ta Nanolamellar Multilayers Fabricated by Cross Accumulative Roll Bonding. *Acta Mater.* **2016**, *110*, 341–351. [CrossRef]

27. Kale, C.; Srinivasan, S.; Hornbuckle, B.C.; Koju, R.K.; Darling, K.; Mishin, Y.; Solanki, K.N. An Experimental and Modeling Investigation of Tensile Creep Resistance of a Stable Nanocrystalline Alloy. *Acta Materialia* **2020**, *199*, 141–154. [CrossRef]

28. Darling, K.A.; Roberts, A.J.; Mishin, Y.; Mathaudhu, S.N.; Kecskes, L.J. Grain Size Stabilization of Nanocrystalline Copper at High Temperatures by Alloying with Tantalum. *J. Alloys Compd.* **2013**, *573*, 142–150. [CrossRef]

29. Tran, A.-S. Phase Transformation and Interface Fracture of Cu/Ta Multilayers: A Molecular Dynamics Study. *Eng. Fract. Mech.* **2020**, *239*, 107292. [CrossRef]

30. Chen, J.; Mathaudhu, S.N.; Thadhani, N.; Dongare, A.M. Unraveling the Role of Interfaces on the Spall Failure of Cu/Ta Multilayered Systems. *Sci. Rep.* **2020**, *10*, 208. [CrossRef]

31. Li, M.; Chang, Y. Improving Tensile Property and Thermal Stability of the Cu-Ta Alloy by Alloying with Cr. *J. Alloys Compd.* **2022**, *905*, 164181. [CrossRef]

32. Wang, J.; Shi, J.; Lu, Y.; Jin, G.; Wang, J.; Jiang, Y.; Zhou, Q. Deformation Evolution of Cu/Ta Nanoscale Multilayer during Nanoindentation by a Molecular Dynamics Study. *Surf. Coat. Technol.* **2022**, *441*, 128562. [CrossRef]

33. Hornbuckle, B.C.; Solanki, K.; Darling, K.A. Prolonged High-Temperature Exposure: Tailoring Nanocrystalline Cu–Ta Alloys against Grain Growth. *Mater. Sci. Eng. A* **2021**, *824*, 141818. [CrossRef]

34. Han, L.; Liu, Z.; Yu, L.; Ma, Z.; Huang, Y.; Liu, Y.; Wang, Z. Effect of WC Nanoparticles on the Thermal Stability and Mechanical Performance of Dispersion-Reinforced Cu Composites. *Scr. Mater.* **2023**, *222*, 115030. [CrossRef]

35. Feng, J.; Song, K.; Liang, S.; Guo, X.; Li, S. Mechanical Properties and Electrical Conductivity of Oriented-SiC-Whisker-Reinforced Al_2O_3/Cu Composites. *J. Mater. Res. Technol.* **2022**, *20*, 1470–1480. [CrossRef]

36. Pan, Y.; Xiao, S.; Lu, X.; Zhou, C.; Li, Y.; Liu, Z.; Liu, B.; Xu, W.; Jia, C.; Qu, X. Fabrication, Mechanical Properties and Electrical Conductivity of Al_2O_3 Reinforced Cu/CNTs Composites. *J. Alloys Compd.* **2019**, *782*, 1015–1023. [CrossRef]

37. Li, W.; Dong, H. Effect of Nano-Y_2O_3 on Microstructure and Mechanical Properties of W–Ni–Cu Alloys. *Mater. Res. Express* **2018**, *5*, 106503. [CrossRef]

38. Mu, Z.; Geng, H.-R.; Li, M.-M.; Nie, G.-L.; Leng, J.-F. Effects of Y_2O_3 on the Property of Copper Based Contact Materials. *Compos. Part B Eng.* **2013**, *52*, 51–55. [CrossRef]

39. Zhuo, H.; Tang, J.; Ye, N. A Novel Approach for Strengthening $Cu–Y_2O_3$ Composites by in Situ Reaction at Liquidus Temperature. *Mater. Sci. Eng. A* **2013**, *584*, 1–6. [CrossRef]

40. Liu, S.; Li, L.; Zhou, M.; Liang, S.; Zhang, Y.; Huang, J.; Tian, B.; Geng, Y.; Liu, Y.; Jia, Y.; et al. Preparation and Properties of Graphene Reinforced $Cu/_{0.5}CeO_{230}$Cr Electrical Contact Materials. *Vacuum* **2022**, *195*, 110687. [CrossRef]

41. Pethő, D.; Kurusta, T.; Kristály, F.; Mikó, T.; Gácsi, Z. The Effect of Ball to Powder Ratio on the Processing of a Novel Mo-Cu-Al$_2$O$_3$ Composite. *Int. J. Refract. Met. Hard Mater.* **2021**, *101*, 105657. [CrossRef]

42. Zhou, Y.; Gan, M.; Yu, W.; Chong, X.; Feng, J. First-Principles Study of Thermophysical Properties of Polymorphous YTaO$_4$ Ceramics. *J. Am. Ceram. Soc.* **2021**, *104*, 6467–6480. [CrossRef]

43. Zhang, F.; Zhang, G.; Yang, L.; Zhou, Y.; Du, Y. Thermodynamic Modeling of YO$_{1.5}$-TaO$_{2.5}$ System and the Effects of Elastic Strain Energy and Diffusion on Phase Transformation of YTaO$_4$. *J. Eur. Ceram. Soc.* **2019**, *39*, 5036–5047. [CrossRef]

44. Flamant, Q.; Gurak, M.; Clarke, D.R. The Effect of Zirconia Substitution on the High-Temperature Transformation of the Monoclinic-Prime Phase in Yttrium Tantalate. *J. Eur. Ceram. Soc.* **2018**, *38*, 3925–3931. [CrossRef]

45. Yang, W.; Ye, F.; Yan, S.; Guo, L. The Corrosion Behaviors of Thermal Barrier Material of M-YTaO$_4$ Attacked by CMAS at 1250 °C. *Ceram. Int.* **2020**, *46*, 9311–9318. [CrossRef]

46. Lepple, M.; Ushakov, S.V.; Lilova, K.; Macauley, C.A.; Fernandez, A.N.; Levi, C.G.; Navrotsky, A. Thermochemistry and Phase Stability of the Polymorphs of Yttrium Tantalate, YTaO$_4$. *J. Eur. Ceram. Soc.* **2021**, *41*, 1629–1638. [CrossRef]